Catalysis Today 172 (2011) 34–40

Contents lists available at ScienceDirect

Catalysis Today

journal homepage: www.elsevier.com/locate/cattod

Evaluation of sulfated tin oxides in the esterification reaction of free fatty acids

J.I. Moreno[a], R. Jaimes[a], R. Gómez[b], M.E. Niño-Gómez[a,*]

[a] Universidad Industrial de Santander, Centro de Investigaciones en Catálisis, Km 2 vía al Refugio, Piedecuesta, Santander, Colombia
[b] Universidad Autónoma Metropolitana-Iztapalapa, San Rafael Atlixco No 186, México 09340, DF, Mexico

ARTICLE INFO

Article history:
Received 1 December 2010
Received in revised form 2 February 2011
Accepted 11 March 2011
Available online 7 May 2011

Keywords:
XRD sulfated tin oxides
Solid superacid
Acidity of Hammett
Esterification of free fatty acids
Sulfated tin oxides acidity

ABSTRACT

Sulfated tin oxides (SO_4^{2-}/SnO_2) with different SO_4^{2-} contents (0.15, 0.3 and 0.45 wt%) were synthesized from hydroxylated tin oxide obtained by the precipitation method, followed by ion exchange of the OH groups with SO_4^{2-} species using a sulfuric acid solution. In samples annealed at 673, 773 and 873 K the characterization of the solids was made by XRD, FT-IR and nitrogen adsorption. The strength and number of acid sites were determined by titration with n-butylamine using Hammett indicators an acid strength of $Ho < -8.2$ was found. Sulfated tin oxides were tested in the esterification reaction of free fatty acids with ethanol (molar ratio 1:10), at 353 K. XRD profiles showed that the sulfating inhibits the SnO_2 crystal growth. The SO_4 species remained strongly bonded at the SnO_2 surface stabilizing its crystallite size against sintering and it acts as a structure porogen director mediating nanoparticle growth and assembly yielding a mesostructured form of SnO_2 with wormhole morphology and high thermal stability. The conversion of oleic acid increases with the increase of surface acidity showing a maximum when the sulfate content and calcination temperature were 0.3 wt% and 773 K, respectively. Regeneration through heating the SO_4^{2-}/SnO_2 with the highest activity for 4 h allows it for reuse without losing of its catalytic activity.

Published by Elsevier B.V.

1. Introduction

Biodiesel consists in a mixture of alkyl esters of fatty acids formed by esterification and transesterification of vegetable oils or animal fats with methanol or ethanol [1,2]. The rate of the transesterification reaction is faster employing a base catalyst, and for this reason the industrial process uses, as catalysts, alkaline hydroxides or methoxides dissolved in methanol, under homogeneous conditions. Basic catalysts are on the other hand not favorable for the production of fatty acids esters owing to the disadvantages such as high sensitivity of the catalysts to water and free fatty acids, and formation of soap [3,4]. Formation of soap lowers the yield of esters and makes the separation of esters difficult. Besides, the base catalyzed reaction requires the use of expensive refined oils that should have low free fatty acids content (inferior to 0.5 wt%) [5,6]. In this way alternative solid base catalysts such as Mg/M (M = Al and Ca) [7], CaO stabilized in siliceous SBA-15 [8], and CaO/ZnO is a very active catalysts prepared from calcium zincate dihydrate as precursor [9] have been recently reported. Among the variety of basic solid catalysts that have been tested, activated CaO is one of the most useful. This catalyst, although affected by some leaching from dissolution of its components, can be reused for several runs without significant loss of activity. Recently, we have found that mixing activated CaO with biodiesel in a proportion of a few grams of biodiesel per gram of solid catalyst result in a notable protection of the activated CaO against poisoning by atmospheric CO_2 and H_2O that may occur during handling of the solid. Small amounts of MG and DG present in the biodiesel were found to be the origin of the increase of the reaction rate. IR studies demonstrated that the glycerol formed in situ during the pretreatment of the biodiesel–CaO reacted with the surface forming very active Ca-glyceroxide [10].

The homogeneous and heterogeneous catalysts are also employed for esterification reactions of free fatty acids for the production of fatty acids esters. Among the homogeneous catalysts sulfuric acid, methane sulfonic acid, p-toluene sulfonic acid are the most common acid catalysts. In spite of several advantages, homogeneous catalysts have some limitations which include problem in recovering the catalysts, disposal of toxic wastes formed during reactions, separation of the products, and loss of catalysts. So, an effective environmentally benign, low cost production of biodiesel extensively demands solid heterogeneous catalysts. The recent works on the esterifications of free fatty acids to produce biodiesel involve the use of different heterogeneous inorganic catalysts such as, zeolites [11], heteropolyacids [12], ion exchange resin [13], carbon based material [14], sulfated ZrO_2 [15], sulfated TiO_2 [16], sulfated SnO_2 [17], and $Nb_2O_5{\cdot}5H_2O$ [18], WO_3/ZrO_2 [19], tungstophosphoric acid [20], tungstosilicic acid

* Corresponding author. Tel.: +57 7 6349069; fax: +57 7 6349069.
E-mail addresses: gomr@xanum.uam.mx (R. Gómez), marenino@yahoo.com, marthan@uis.edu.co (M.E. Niño-Gómez).

0920-5861/$ – see front matter. Published by Elsevier B.V.
doi:10.1016/j.cattod.2011.03.052

[21] and molybdophosphoric acid immobilized on SiO_2 [22], SnO [23]. Since the discovery of the M41S materials [24], by supramolecular assembly, several efforts have been focused to extend this pathway to the synthesis of a variety of mesoporous metal oxide and sulfide compositions in order to increase the exposed surface area. Mesostructured forms of tin oxide [25] have been obtained by hydrolysis of inorganic precursors in the presence of cationic, anionic and neutral surfactants as structural directors. In most cases, SnO_2 is not stable to the surfactant removal and the mesostructure collapsed upon calcinations of the template or attempted removal by ion exchange in solution. To increase the mesostructure stability against surfactant removal, several groups have proposed the synthesis of mesoporous metal oxides by using an anionic surfactant with phosphate, sulfate or sulfonate headsurfactant template [26–29]. The sulfate or phosphate headgroups remain bonded to the surface, stabilizing the mesostructured walls and increasing its thermal stability. In fact, it has been reported that functionalization of the oxide surface by sulfate preserves the textural properties of oxides [30,31].

On the other hand the use of solid acid catalysts offers many advantages; they have especially the ability to simultaneously catalyze the esterification and transesterification reactions, and many of them have been already reported in the literature to be active in both reactions. Many studies have been reported concerning sulfated metal oxides as superacids, where sulfated zirconia (SO_4^{2-}/ZrO_2) which exhibits high catalytic activities for various reactions is a typical example [32], it shows strongest superacidity; its acid strength is lower than −16 on the Hammett function scale [4]. Commonly, the superacids have been prepared by following the next steps: (i) preparation of amorphous metal oxide gels as precursors; (ii) treatment of the gels with sulfate ion by exposure to a H_2SO_4 solution or by impregnation with $(NH_4)_2SO_4$; (iii) calcination of the sulfated materials at a high temperature in air. In this way sulfated tin oxide (SO_4^{2-}/SnO_2) is one of the more promising acids solids with strongest acidity. It has been reported that its acid strength can be comparable to that of SO_4^{2-}/ZrO_2 [33]. Temperature programmed desorption (TPD) of pyridine [34] and temperature-programmed reaction of adsorbed furan [35] indicate the possibility that SO_4^{2-}/SnO_2 has an acid strength higher than that of SO_4^{2-}/ZrO_2. Nevertheless, papers concerning the study of SO_4^{2-}/SnO_2 catalysts have been scarcely reported [36–38] because of the complexity in their preparation, in particular owing to the difficulty to obtain the oxide gels from its salts.

However, to our knowledge the mesoporous SO_4^{2-}/SnO_2 has not yet been explored as a catalyst in esterifications reactions of free fatty acids. In this work, thermally stable mesostructured tin oxide was synthesized by functionalization of SnO_2 nanoparticles obtained directly by precipitation of chloride precursor with ammonia, without surfactant, and sulfated with sulfuric acid. The SO_4^{2-}/SnO_2 catalysts showed activity during the esterification reaction of free fatty acids with ethanol at 373 K. Regeneration through heating of the SO_4^{2-}/SnO_2-0.3–773 K used mesoporous catalyst allowed it for reuse without losing of its catalytic activity.

2. Experimental

2.1. Reagents

Stannous chloride at 99% was procured from Mallinckrodt. Ammonium hydroxide at 25 vol%, ammonium acetate and oleic acid at 79% were obtained from Carlo Erba. Red methyl, blue thymol, violet crystal, antraquinone, sulfuric acid 95% and n-butylamine were supplied by Merck. Ethanol 99.9% was selected from J.T. Baker.

2.2. Preparation of the SO_4^{2-}/SnO_2 catalysts

The SO_4^{2-}/SnO_2 catalysts were prepared following the method described elsewhere [39,40]. In a typical synthesis, 22.82 g of $SnCl_2{\cdot}2H_2O$ (99% purity) were dissolved in 600 mL of distilled water, then aqueous solution was added dropwise a NH_4OH (25 vol%) solution with continuous vigorous stirring until the solution reach a final pH 8. The pale yellow gel type precipitate obtained was filtered and suspended in a 4% CH_3COONH_4 solution during 30 min. Then, the $Sn(OH)_2$ XH_2O gels were impregnated with the appropriate amount of a 3 M H_2SO_4 solution to obtain 0.15, 0.3 and 0.45 wt% of sulfate. After, the gels were dried at 373 K for 24 h and calcined at 673 K, 773 K and 873 K for 3 h. For identification the solids were labeled as SO_4^{2-}/SnO_2 0.15 K, 0.3 K and 0.45 K, where the figures indicate the SO_4^{2-} content and K the calcinations temperatures. A blank was prepared with the $SnCl_2{\cdot}2H_2O$ precursor but omitting the sulfation step.

2.3. Characterization

2.3.1. Specific surface area

Nitrogen adsorption isotherms were obtained on the tin oxide and sulfated tin oxides, using an equipment Nova 1200 mark Quantachrome. The surface area was calculated with the BET equation and the mean pore size diameter was calculated by using the BJH method.

2.3.2. FTIR spectroscopy

The IR absorption spectra were obtained with a Bruker model Tensor 27 equipment in the range of 4000–400 cm^{-1}, using KBr powders.

2.3.3. X-ray diffraction

The SO_4^{2-}/SnO_2 catalysts were characterized by powder X-ray diffraction with a RIGAKU, model D/MAX IIIB diffractometer. A Cu target was used as X-ray source at 40 kV and 20 mA. The samples were recorded in the $2 < 2\theta < 70$ range with a step time of 1 s and a step size of 0.02° (2θ). The crystallite size (nm) was calculated from the broadening of the strongest peak of SnO_2, peak (1 1 0) at $2\theta = 26.64$, using Scherrer equation [41].

$$D = \frac{k\lambda}{\beta \cos \theta}$$

where k is the crystallite shape constant (≈1), λ is the radiation wavelength (Å), β is the line breadth (radians) and θ is the Bragg angle.

2.3.4. Thermogravimetric analysis

A Seiko Exstar 6300 thermal analysis instrument was used to study the thermal evolution of the catalyst precursors. The samples were heated from room temperature to 800 °C at a heating rate of 10 °C/min under static air.

2.3.5. Titration method with n-butylamine using Hammett indicators

The surface acidity and acid strength of the catalysts were determined by titration with n-butylamine using the Hammett indicators: red methyl ($Ho \leq +4.8$), blue thymol ($Ho \leq +1.6$), violet crystal ($Ho \leq +0.8$) and antraquinone ($Ho \leq -8.2$). The titration was carried out by dispersing 0.05 g of catalyst in 5 mL of dry benzene; two indicator drops in the benzene solution were then added to the resulting dispersed solution and the titration was done with a solution of n-butylamine 0.01 N. The acidity was calculated in mole of acid sites per gram of catalyst and the acidity strength was expressed in terms of the Hammett acidity (Ho) [42].

2.4. Esterification reaction of free fatty acids

The esterification reactions of free fatty acids were carried out under reflux at 353 K and constant stirring (250 rpm) using an oleic acid at 79%, oleic acid:ethanol molar ratio was of 1:10 and the weight of was 3 wt%. The analysis of the products was made at various time intervals taking the samples from the reactant system during 4 h and analyzed by gas chromatography using an Agilent 6890 gas chromatograph connected to a flame ionization detector (FID) equipped with a HP-InnoWax Polyethyleneglycol capillary column (30 m × 0.320 mm × 0.25 μm). The weight of the used catalyst was 3% over the initial weight.

3. Results and discussion

3.1. Characterization of SO_4^{2-}/SnO_2 by FT-IR spectroscopy

The infrared absorption spectra of tin oxide are shown in Fig. 1. Sulfated tin oxides showed absorption bands in the 1200 cm^{-1} and 900 cm^{-1} region, while those cannot be observed on tin oxide. The bands were assigned to vibrational modes of bidentate sulfate groups on Sn^{4+} cation [17]. The bands at 1044 and 990 cm^{-1} were assigned to asymmetric and symmetric S–O stretching vibrations, respectively [43–45]. The bands at 1622 and 3398 cm^{-1} were associated with the bending and stretching vibrations of the OH group of water molecules on the surface of the solid and with terminal OH which are characteristic of metal oxides, respectively; the band around 610 cm^{-1} corresponds to Sn–O bending vibrations [46]. The FTIR spectra indicates that the S=O group acts as an electron-withdrawing species followed by the inductive effect; thus, the Lewis acid strength of Sn^{4+} becomes stronger.

3.2. XRD study

The effect of sulfate content on the crystallinity of SO_4^{2-}/SnO_2 is shown in Fig. 2. The stabilization of crystallite size by the SO_4 groups bonded to the SnO_2 surface can be clearly observed by comparing the XRD patterns of the sulfated tin oxide annealed at 773 K and without sulfate. Tin oxide shows a patterns characteristic of pure SnO_2 phase with tetragonal cassiterite structure at 2θ = 26.63, 33.82 and 51.77 (PDF-2 of ICDD). The cassiterite phase was also showed

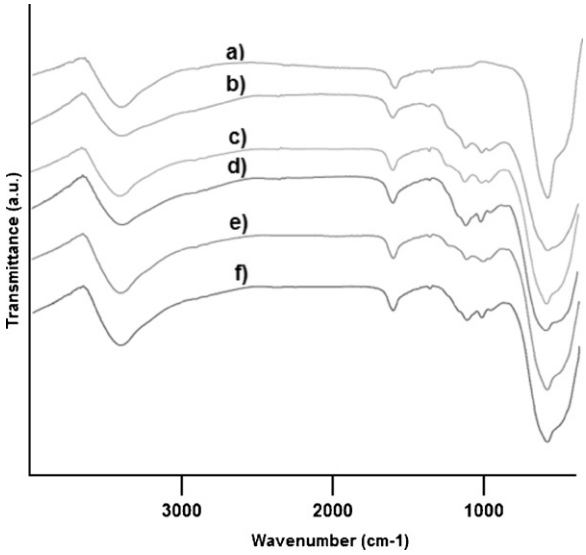

Fig. 1. FT-IR spectra of tin oxide, (a) SnO_2-773 and sulfated tin oxide: (b) SO_4^{2-}/SnO_2 0.45–673 K, (c) SO_4^{2-}/SnO_2 0.45–773 K, (d) SO_4^{2-}/SnO_2 0.45–873 K, (e) SO_4^{2-}/SnO_2 0.3–773 K and (f) SO_4^{2-}/SnO_2 0.15–773 K.

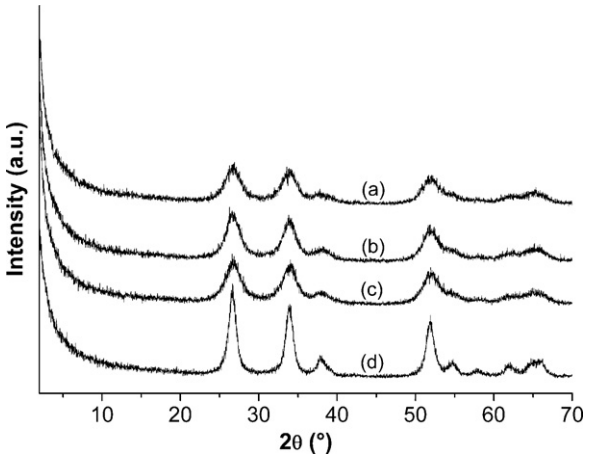

Fig. 2. X-ray diffraction profiles of tin oxides annealed at 773 K: (a) SO_4^{2-}/SnO_2 0.45, (b) SO_4^{2-}/SnO_2 0.3 (c) SO_4^{2-}/SnO_2 0.15 and (d) SnO_2.

by the sulfated tin oxides; however the intensity of the bands gradually decreases. The decrease in the crystallite size can be explained by the hypothesis that the bulky sulfate groups on the surface of SnO_2 particles prevent their glomeration during annealing. The width of the reflections is considerably broadened, indicating a small crystalline domain size, Khder et al. [41] observed similar patterns. To see the effect of sulfate content on the crystallinity of the samples quantitatively, their mean crystallite sizes was calculated from the broadening of the strongest peak of SnO_2, peak (1 1 0) at 2θ = 26.6 and based on Scherrer equation, Table 1. The crystallite size of pure SnO_2 (II) started at 7.3 nm, addition of sulfate was associated with a notable decrease of crystallite size to reach 3.4 nm for SO_4/SnO_2-0.45–673. At 773 K the SO_4 groups remain bonded at the surface and inhibit the growth of the SnO_2 crystallites, such as have been done by sulfating of other transition metal oxides like TiO_2, ZrO_2, Fe_2O_3, and so forth [47–49]. Gutiérrez-Báez [50] by XRD Rietveld analysis found that crystallite size increased considerable when the SO_4 groups were removed from SnO_2 surface.

The effect of annealing temperature on the crystallinity of SO_4^{2-}/SnO_2 is shown in Fig. 3. A progressive narrowing of the main lines as function of the temperature can be observed showing a small increase of the crystallite size [22]. This small sintering of crystalline SnO_2, can be attributed to the loss of some sulfate groups bonded to SnO_2 [17]. At 673 K, 773 K and 873 K the sulfate groups remain bonded at the surface of the solid and inhibit the growth of SnO_2 crystallites. Recently, Toledo-Antonio et al. [51] had reported that in sulfated tin oxide the hydroxyls remaining in the bulk of the crystallite generate a structure poorly crystallized with a large amount of tin vacancy sites. The fresh sulfated SnO_2 sample, which has SO_4^{2-} and also hydroxyls in it, presented a large amount of tin vacancy sites (≈50%) which decreased to 22.8% while annealing the sample at 773 K. However, when SO_4^{2-} was eliminated, the tin vacancy sites drastically decreased at 5.6 and 4.4% when the samples were annealed at 973 K and 1273 K, respectively.

Table 1
Crystallite size of the SnO_2 and SO_4^{2-}/SnO_2 obtained from XDR using Scherrer equation.

Catalyst	Crystallite size (nm)	I(1 1 0) peak
SnO_2-773	7.3	183.4
SO_4^{2-}/SnO_2-0.45–873	4.5	92.9
SO_4^{2-}/SnO_2-0.3–773	4.3	92.9
SO_4^{2-}/SnO_2-0.15–773	3.9	80.2
SO_4^{2-}/SnO_2-0.45–773	3.8	69.7
SO_4^{2-}/SnO_2-0.45–673	3.4	55.4

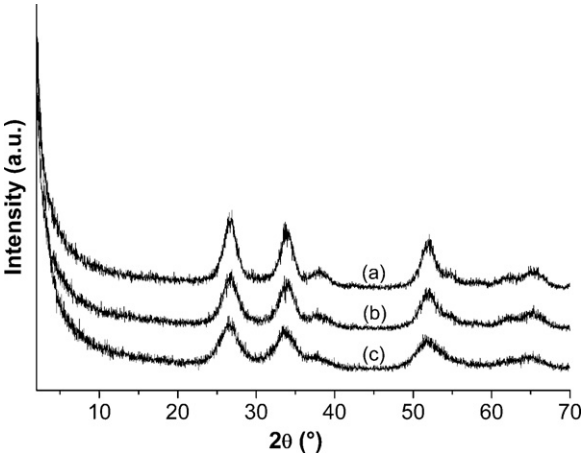

Fig. 3. X-ray diffraction profiles of SO_4^{2-}/SnO_2-0.45 samples annealed at (a) 873 K, (b) 773 K and (c) 673 K.

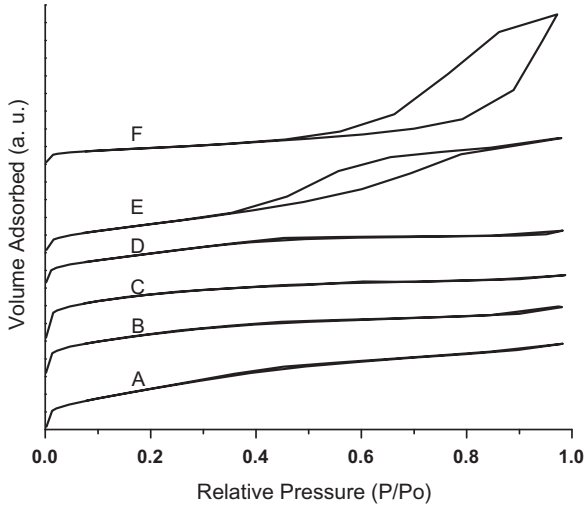

Fig. 4. The isotherms of the SO_4^{2-}/SnO_2 catalysts; (A) SO_4^{2-}/SnO_2-0.45–873 K; (B) SO_4^{2-}/SnO_2-0.15–773 K; (C) SO_4^{2-}/SnO_2-0.45–673 K; (D) SO_4^{2-}/SnO_2-0.3–773 K; (E) SO_4^{2-}/SnO_2-0.45–773 K; and (F) SnO_2-773 K.

3.3. Specific surface area of catalysts

It is clear that interaction between SO_4^{2-} and SnO_2 stabilizes the SnO_2 against sintering producing a strongly deformed structure. However, it is interesting to know how the presence of SO_4^{2-} on the SnO_2 surface affects the specific surface area and pore size distribution, which are important parameters to take into account when this material is used as ion host or as catalyst. The specific surface areas obtained from the nitrogen adsorption isotherms are reported in Table 2. The results showed that for the sulfated samples the BET areas are higher in comparison with SnO_2. The specific surface area of tin oxide was 62 m^2/g and for the sulfated tin oxides were 92, 99 and 88 m^2/g for the catalysts (0.45% SO_4^{2-}) annealed at 673 K, 773 K and 873 K respectively, while for samples annealed at 773 K with 0.15, 0.3 and 0.45 wt% SO_4^{2-} the BET areas were 85, 87 and 99 m^2/g, respectively. Thus, for sulfated samples the annealing temperature as well as the sulfate content have only marginal effects in the BET areas, pore volume and pore diameter. The important diminution in the specific surface areas (289–143 m^2/g) on nanocrystalline SnO_2 particles obtained by the sol–gel method as function of the annealing temperature reported by Zhang and Gao [22] is not observed in the present work i.e. the sulfated ion strongly diminishes the sintering of SnO_2. Recently, Sarkar et al. [52] developed a mesoporous SnO_2/WO_3 catalyst with surface area, pore volume and pore size of 130 m^2/g, 0.198 cm^3/g and 3.9 nm, respectively.

The results of analysis thermo gravimetric (TGA) are showed in Table 2. These results show that the amount of sulfate groups coordinated at tin oxide decreases with the calcination temperature indicating loss of sulfate groups. At 773 K the amount of sulfated groups increased with the amount added.

The isotherms observed in the SO_4^{2-}/SnO_2 catalysts annealed at 723 K, Fig. 4, corresponded to type IV in the Brunauer Deming Deming and Teller (BDDT) classification often observed in porous solid. When the annealing temperature was increased from 673 to 873 K, the hysteresis loop of the nitrogen isotherms moved to higher relative pressure with the consequent increase in pore diameter and decrease in the corresponding BET surface area. The changes in nitrogen adsorption isotherms were due to the structural transition from a wormhole mesotructure to a nanocrystalline material which had interparticle mesoporosity. The wormhole structure template by the SO_4^{2-} was retained. In the sulfated sample annealed between 623 at 823 K, the crystallite size did not change, suggesting that SO_4 species remain bonded at the surface, stabilizing it against sintering.

The above results suggest that the interaction between SO_4^{2-} and SnO_2 crystallites not only stabilizes the crystallites in lower dimensions, but it remains at the SnO_2 surface inhibiting the crystallite aggregation and acts as a structure porogen director mediating nanoparticle growth and assembly. Also the sulfate groups remain bonded to the surface, stabilizing the mesostructured walls and increasing its thermal stability. In fact, several efforts have been focused to obtain mesostructured forms of SnO_2,

Table 2
Textural properties of the SnO_2 and SO_4^{2-}/SnO_2 catalysts.

Catalyst	Specific surface area [m^2/g]	Pore volume [cm^3/g]	Pore diameter [Å]	[TGA] mmol SO_3/g catalyst
SnO_2-773	62	0.051	70	
SO_4^{2-}/SnO_2-0.45–773	99	0.054	25	0.201
SO_4^{2-}/SnO_2-0.45–873	88	0.052	28	0.137
SO_4^{2-}/SnO_2-0.3–773	87	0.050	28	0.194
SO_4^{2-}/SnO_2-0.15–773	85	0.060	28	0.129
SO_4^{2-}/SnO_2-0.45–673	92	0.060	26	0.194

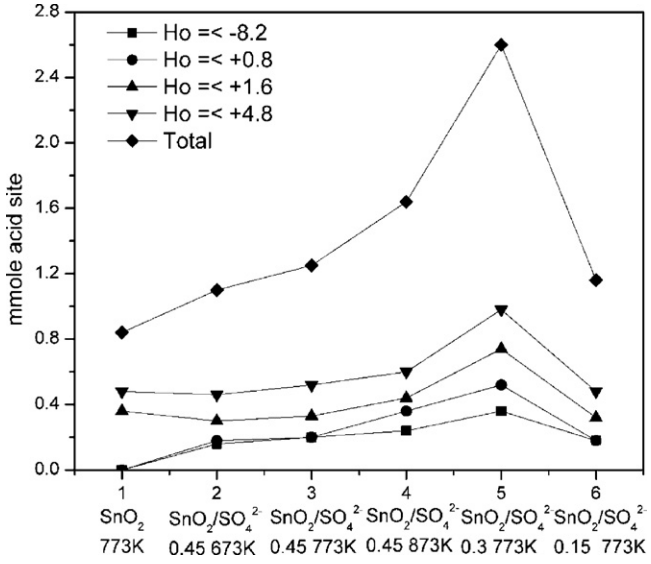

Fig. 5. The total number of acid sites/g for the SnO_2 and SO_4^{2-}/SnO_2 catalysts using Hammett indicators: ▼ red methyl, ▲ blue thymol, ● violet crystal and ■antraquinone.

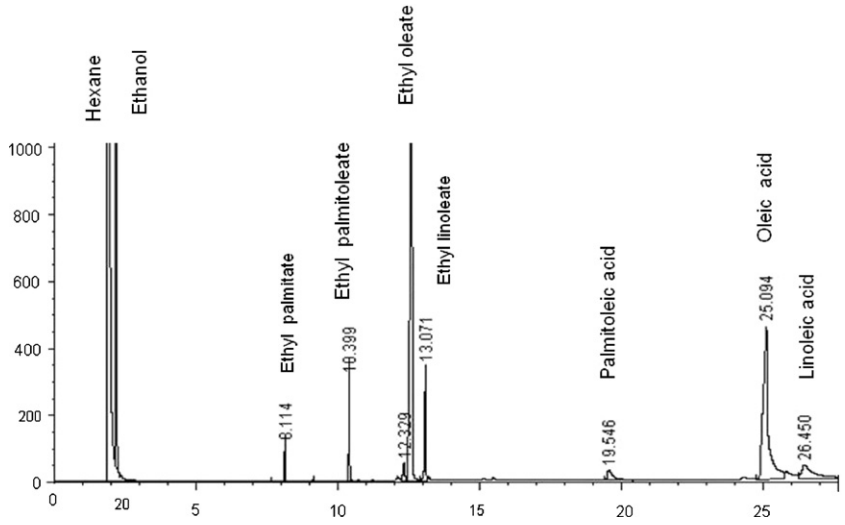

Fig. 6. Chromatogram of the reaction mixture obtained during the esterification of free fatty acids with SO_4^{2-}/SnO_2-0.3–773 K catalyst after 4 h.

using ionic and neutral surfactants as a structure porogen director. However, their thermal stability was very low and the mesostructure collapsed after removing the surfactant by annealing at 573 K [53].

3.4. Acid properties of acid sites in SnO_2 and SO_4^{2-}/SnO_2

The acid strength and amount of acid sites is presented in Fig. 5. This result clearly shows a remarkable increase in acidity when sulfated ion is incorporated in to the sample. The total number of acid sites/g for the SnO_2 and SO_4^{2-}/SnO_2 catalysts was calculated using Hammett indicators: red methyl ($Ho \leq +4.8$), blue thymol ($Ho \leq +1.6$), violet crystal ($Ho \leq +0.8$) and antraquinone ($Ho \leq -8.2$). The titration with n-butylamine shows that tin oxide has a low number of acid sites, while on samples with 0.45% SO_4^{2-} a gradual increase of the total number of acid sites as a function of annealing temperature can be seen: it varies from 1.1 to 1.64 mmol/g for the samples thermally treated at 673 and 873 K respectively. For the samples annealed at 773 K with different sulfate content a maximum on acidity was observed on the SO_4^{2-}/SnO_2-0.3–773 sample (2.60 mmol/g), after it decreases on the SO_4^{2-}/SnO_2-0.45–773 catalyst (1.25 mmol/g). The low acid strength distribution over the surface of the tin oxide ($Ho \leq +1.6$) and the higher acid strength ($Ho \leq -8.2$) showed by the sulfated tin oxide samples is attributed to the strong interactions between the sulfate ions and the cassiterite phase of tin oxide. This result agrees with the amount of sulfate groups coordinate at tin oxide, showed in Table 2.

3.5. Catalytic evaluation

Esterification of oleic acid at 79% with ethanol was studied over the 3.0 wt% SO_4^{2-}/SnO_2 catalysts at a reaction temperature of 353 K. The reactants molar ratio (oleic acid:ethanol) was maintained at 1:10. Fig. 6 shows the chromatogram of the reaction mixture obtained during the esterification of free fatty acids with SO_4^{2-}/SnO_2-0.3–773 catalyst after 4 h of reaction. The ethyl esters were the only reaction products indicating 100% selectivity at ethyl oleate. The effect of sulfate content and calcination temperature on structure, acidity and catalytic activity of tin oxide is presented in Fig. 7. The conversion of oleic acid increased with the total number of acid sites of catalyst. Total number of acid sites was maximum when the sulfate content and calcinations temperature was 0.3 wt% and 773 K. These results indicate that the activity is attributed to acid sites. Similar behavior was observed by Khder et al. [41] during the esterification of acetic acid with amyl alcohol at 523 K using with a molar ratio acetic acid:amyl alcohol of 1:2. The catalytic activity over 0–30 wt% SO_4^{2-}/SnO_2 catalysts annealed at 673, 823, and 1023 K was maximum when the sulfate content and calcinations temperature was 30 wt% and 823 K, respectively. Recently, Sarkar et al. [52] studied the synthesis of a new, effective and reusable heterogeneous catalyst, mesoporous SnO_2/WO_3 catalyst.

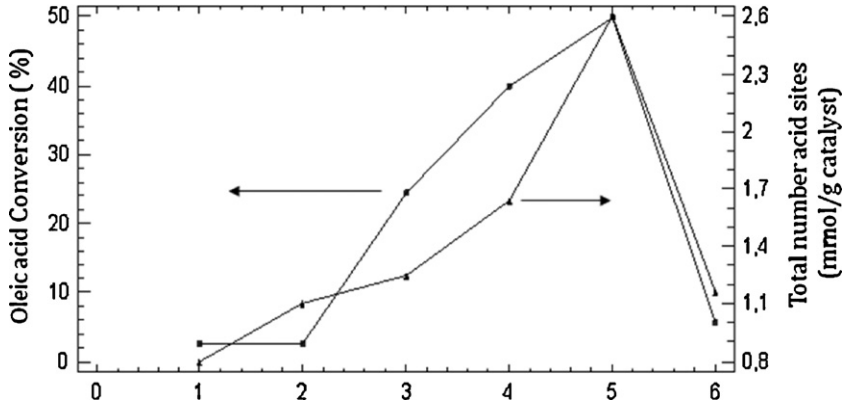

Fig. 7. Catalytic activity and total number of acid sites of the catalysts: (1) SnO_2-773 K, (2) SO_4^{2-}/SnO_2-0.45–673 K, (3) SO_4^{2-}/SnO_2-0.45–773 K, (4) SO_4^{2-}/SnO_2-0.45–873 K, (5) SO_4^{2-}/-SnO_2-0.3–773 K and (6) SO_4^{2-}/SnO_2-0.15–773 K during the esterification reaction of oleic acid with ethanol (molar ratio 1:10) at 353 K, after 4 h of reaction.

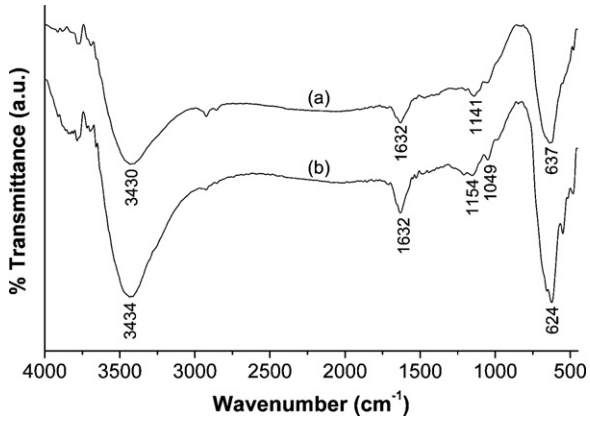

Fig. 8. FT-IR spectra of SO_4^{2-}/SnO_2-0.3–773 K catalyst (a) fresh and (b) used.

The developed mesoporous SnO_2/WO_3 catalyst with surface area of 130 m^2/g and pore size of 3.9 nm exhibited up 90% conversion of oleic acid during 2 h reaction at 353 K with high yield (≈92%) to the ethyl oleate.

3.6. Reusability of catalyst

Fig. 8 shows the infrared absorption spectra of sulfated tin oxide, SO_4^{2-}/SnO_2-0.3–773, fresh and used catalysts. Both spectra showed absorption bands in the 1200 cm^{-1} and 900 cm^{-1} region, corresponding to vibrational modes of bidentate sulfate groups, indicating the presence of sulfate groups in the solid used. Recycling of the catalyst is an important aspect of any industrial process. For this purpose, reusability of the catalyst is tested by carrying out a repeated cycles of the reaction at 353 K, keeping the reactants molar ratio oleic acid:ethanol at 1:10. After performing the reaction over fresh catalyst, the catalyst was washed with hexane and acetone and then was dried at 393 K. The catalyst was reactivated with N_2 at 673 K for 4 h. The reaction was again performed on the reactivated catalyst. It is evident that the activity of the catalyst did not decrease appreciably even after three cycles as shown in Fig. 9. The oleic acid conversion was of 50% and 40% in the fresh and used catalysts after 4 h. This result indicates that a heterogeneous catalytic process is happening. The leaching of the sulfates species produces homogeneous catalytic reactions with 100% oleic acid conversion in 2 h of reaction. In this case does not reach the leaching total sulfates groups. These results are comparable with sulfated tin oxide used in other system catalytic [41,53].

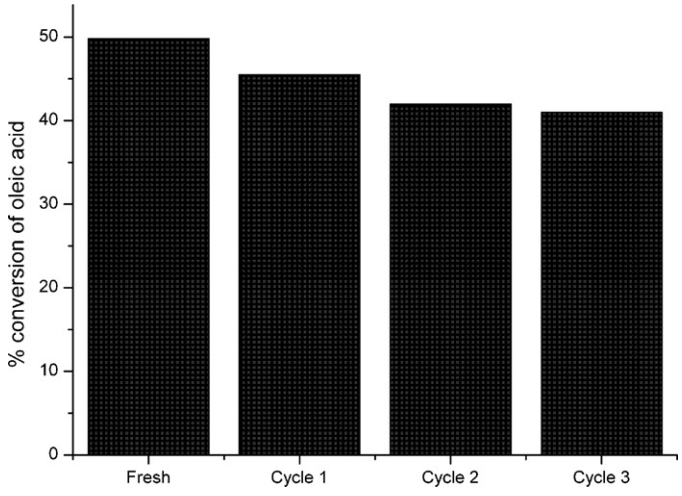

Fig. 9. Conversion of oleic acid obtained with the fresh and used SO_4^{2-}/SnO_2-0.3–773 K catalyst during the esterification reaction with ethanol (molar ratio 1:10) at 353 K, after 4 h of reaction.

4. Conclusions

The conditions of preparation of sulfated tin oxide are determinant on the structure, acidity and catalytic activity. The stabilization of crystallite size by the SO_4 groups bonded to the SnO_2 surface was clearly observed. At 673, 773 and 873 K the sulfate groups remain bounded to the surface of the solid and inhibit the growth of SnO_2 crystallites. The sulfate groups increase the specific surface area, stabilizing the mesostructured walls and increasing its thermal stability. There is a direct correlation between the amount total of acid sites and the catalytic activity of sulfated tin oxide in the esterification reaction of oleic acid. The conversion of oleic acid and the surface acidities was maximum when the sulfate content and calcination temperature was 0.3 wt.% and 773 K. Sulfated tin oxides are solids acids catalysts of low pollutant and promisourios catalysts in the production of alternative ethyl esters from free fatty acids.

Acknowledgements

The authors acknowledge the economic support given by COLCIENCIAS, 110245221393 project and the Industrial University of Santander. The CONACYT-Mexico support given to the CB 62053 project.

References

[1] H. Fukuda, A. Kondo, H. Noda, J. Biosci. Bioenerg. 92 (2001) 405–416.
[2] F. Ma, M.A. Hanna, Bioresour. Technol. 70 (1999) 1–15.
[3] E. Lotero, Y. Lui, D.E. López, K. Suwannakarn, D.A. Bruce, J.G. Goodwin, Ind. Eng. Chem. Res 44 (2005) 5353–5363.
[4] D.E. Lopez, J.G. Goodwin Jr., D.A. Bruce, E. Lotero, Appl. Catal. A: Gen. 295 (2005) 97–105.
[5] D.A.C. Ferreira, M.R. Meneghetti, S.M.P. Meneghetti, C.R. Wolf, Appl. Catal. A: Gen. 317 (2007) 58–71.
[6] H.J. Kim, B.S. Kang, M.J. Kim, D.K. Kim, J.S. Lee, K.Y. Lee, EuropaCat IV, vol. B1, Innsbruck, Austria, 2003, p. 089.
[7] M.C.G. Alburquerque, I. Jiménez-Urbistondo, J. Santamaría-González, J.M. Mérida-Robles, R. Moreno-Tost, E. Rodríguez-Castellón, A. Jiménez-López, D.C.S. Azevedo, C.L. Cavalcante Jr., P. Maireles-Torres, Appl. Catal. A: Gen. 334 (2008) 35–43.
[8] J.M. Rubio-Caballero, J. Santamaria-Gonzalez, J. Merida-Robles, R. Moreno-Tost, Jimenez-Lopez, P. Maireles-Torres, Appl. Catal. B: Environ. 91 (2009) 339–346.
[9] M. Canakei, J.V. Germen, Trans. Am. Soc. Agric. Eng. 44 (2001) 1429–1436.
[10] M. López Granados, A.C. Alba-Rubio, F. Vila, D. Martín Alonso, R. Mariscal, J. Catal. 276 (2010) 229–236.
[11] A.A. Kiss, A.C. Dimian, G. Rothenberg, Adv. Synth. Catal. 348 (2006) 75–81.
[12] H. Matsuda, T. Okuhara, Catal. Lett. 56 (1998) 241–243.
[13] T. Okuhara, Catal. Today 73 (2002) 167–176.
[14] A. Takagaki, M. Toda, M. Okamura, J.N. Kondo, S. Hayashi, K. Domen, M. Hara, Catal. Today 116 (2006) 157–161.
[15] D.E. Lopez, J.G. Goodwin Jr., D.A. Bruce, S. Furuta, Appl. Catal. A: Gen. 339 (2008) 76–83.
[16] J. Ni, F.C. Meunier, Appl. Catal. A: Gen. 333 (2007) 122–130.
[17] S. Furuta, H. Matsuhashi, K. Arata, Appl. Catal. A: Gen. 269 (2004) 187–191.
[18] A.A. Kiss, A.C. Dimian, G. Rothenberg, Energy Fuels 22 (2008) 598–604.
[19] Y.-M. Park, D.-W. Lee, D.-K. Kim, J.-S. Lee, K.-Y. Lee, Catal. Today 131 (2008) 238–243.
[20] J.C. Juan, J. Zhang, M.A. Yarmo, J. Mol. Catal. A: Chem. 267 (2007) 265–271.
[21] C.S. Caetano, I.M. Fonseca, A.M. Ramos, J. Vital, J.E. Castenheiro, Catal. Commun. 9 (2008) 1996–1999.
[22] J. Zhang, L. Gao, J. Solid State Chem. 177 (2004) 1425–1430.
[23] Y. Wang, Y. Lui, C. Lui, Energy Fuels 22 (2008) 2203–2206.
[24] J.S. Beck, J.C. Vartuli, W.J. Roth, M.E. Leonowicz, C.T. Kresge, K.D. Schmitt, C.T.-W. Chu, D.H. Olson, E.W. Sheppard, S.B. McCullen, J.B. Higgins, J.L. Schlenker, J. Am. Ceram. Soc. 114 (1992) 10834–10843.
[25] F. Cheng, Z. Shi, M. Lui, J. Chem. Soc. Chem. Commun. 20 (2000) 2095–2096.
[26] M.S. Wong, J.Y. Ying, Chem. Mater. 10 (1998) 2067–2077.
[27] U. Ciesla, M. Froba, G. Stucky, F. Schuth, Chem. Mater. 11 (1999) 227–234.
[28] G. Pacheco, E. Zhao, A. Garcia, A. Sklyarov, J.J. Fripiat, Chem. Commun. 5 (1997) 491–493.
[29] E. Zhao, O. Hernandez, G. Pacheco, S. Hardcastle, J.J. Fripiat, J. Mater. Chem. 8 (1998) 1635–1640.

[30] Y.Y. Huang, T.J. McCarthy, W.M.H. Sachtler, Appl. Catal. A: Gen. 148 (1996) 135–154.
[31] K. Arata, Adv. Catal. 37 (1990) 165–211.
[32] A. Corma, H. Garcia, Catal. Today 38 (1997) 257–308.
[33] K. Arata, Appl. Catal. A: Gen. 146 (1996) 3–32.
[34] H. Matsuhashi, M. Hino, K. Arata, Chem. Lett. (1988) 1027–1028.
[35] H. Matsuhashi, M. Hino, K. Arata, K. Tanabe, H. Hattori, T. Yamaguchi, T. Tanaka (Eds.), Acid-Base Catalysis, Kodansha, Tokyo, 1989, p. 357.
[36] H. Matsuhashi, M. Hino, K. Arata, Appl. Catal. A: Gen. 59 (1990) 205–212.
[37] M.K. Lam, T.K. Lee, R.A. Mohamed, Appl. Catal. B: Environ. 93 (2009) 134–139.
[38] G.W. Wang, H. Hattori, K. Tanabe, Chem. Lett. (1983) 277–280.
[39] H. Matsuhashi, H. Miyazaki, Y. Kawamura, H. Nakamura, K. Arata, Chem. Mater. 13 (2001) 3038–3042.
[40] H. Matsuhashi, H. Miyazaki, K. Arata, Chem. Lett. (2001) 452–453.
[41] S. Khder, E.A. El-Sharkawy, S.A. El-Hakam, A.I. Ahmed, Catal. Commun. 9 (2008) 769–777.
[42] M. Yurdakoc, M. Akc Ay, Y. Tonbul, K. Yurdakoc, Turk. J. Chem. 23 (1999) 319–327.
[43] L. Noda, R. de Almeida, L.F. Probst, N. Goncalves, J. Mol. Catal. A: Chem. 225 (2005) 39–46.
[44] K. Nakamoto, Infrared and Raman Spectra of Inorganic and Coordination Compounds, sixth ed., John Wiley & Sons, Inc., New York, 2009.
[45] S.M. Jung, P. Grange, Catal. Today 59 (2000) 305–312.
[46] J. Navarrete, T. López, R. Gómez, Langmuir 12 (1996) 4385–4390.
[47] A.Y. Jogalekar, R.G. Jaiswal, R.V. Jayaram, J. Chem. Technol. Biotechnol. 71 (1998) 234–240.
[48] A. Corma, A. Martinez, C. Martinez, Appl. Catal. A: Gen. 144 (1996) 249–268.
[49] M. Hino, K. Arata, J. Am. Ceram. Soc. 101 (1979) 6439–6441.
[50] R. Gutiérrez-Báez, J.A. Toledo-Antonio, M.A. Cortés-Jácome, P.J. Sebastian, A. Vázquez, Langmuir (2004) 4265–4271.
[51] J.A. Toledo-Antonio, R. Gutiérrez-Báez, P.J. Sebastián, A. Vázquez, J. Solid State Chem. 174 (2003) 241–248.
[52] A. Sarkar, S.K. Ghosh, P. Pramanik, J. Mol. Catal. A: Chem. 327 (2010) 73–79.
[53] L. Qi, J. Ma, H. Cheng, Z. Zhao, Langmuir 14 (1998) 2579–2581.